



Photosensitivity properties of Eu-doped SnS₂ thin films deposited by cost-effective nebulizer spray pyrolysis technique

A. M. S. Arulanantham¹ · P. Mohan Raj² · K. V. Gunavathy³ · M. Rigana Begam⁴ · V. Ganesh⁵ · H. Algarni⁵

Received: 19 January 2022 / Accepted: 14 March 2022 / Published online: 31 March 2022
© The Author(s), under exclusive licence to Springer-Verlag GmbH, DE part of Springer Nature 2022

Abstract

The current research explores the outcome of europium doping on the structure, morphology, electrical conductivity and optoelectronic characteristics of SnS₂ thin films deposited on glass substrates by nebulizer spray technique. X-ray diffraction analysis substantiates the presence of hexagonal structure in both pure and Eu-doped SnS₂ thin films with the highly preferred orientation diffracted from the plane (002). It shows the intensity of the predominant peak is highest for 2% Eu-doped SnS₂ thin film. From the XRD data, the crystallite size was found to be highest for 2% SnS₂:Eu, and same sample showed a less dislocation density of 0.97×10^{15} lines/m² and microstrain of 0.081×10^{-3} /lines² m⁴. The crystallite size first increases with increasing doping concentration of Eu (0–2%), then decreases for higher concentrations. The SEM and AFM micro images reveal the agglomeration of grains at higher Eu concentration. The compositional analysis through EDAX studies supports the presence of Eu, Sn and S. The SnS₂ optical band gap value is found to vary from 2.70 to 2.91 eV as the Eu doping is increased from 2 to 6%. All the SnS₂ thin film samples manifest a n-type conductivity as authenticated from Hall studies and a low resistivity of 4.34×10^{-1} cm with an elevated carrier concentration of 5.43×10^{17} cm⁻³, respectively, was observed for SnS₂:Eu (2 wt%). The same sample established a higher responsivity (41.64×10^{-3} AW⁻¹), competent external quantum efficiency (97.24%), and a better detectivity (40.88×10^8 Jones). Hence, the 2% Eu-doped SnS₂ film is recognized to be best suited for the fabrication of high-speed optoelectronic devices. This paper also discusses a putative mechanism for photo-detector performance under air and UV radiation.

Keywords Europium-doped SnS₂ · Optical studies · Hall-effect measurement · Photosensitivity

1 Introduction

Metal-based semi-conducting chalcogenide thin films have showed considerable promise in the production of optoelectronic devices, solar cells, thermoelectric, and sensor applications in recent years [1–4]. The physical, chemical, and optoelectronic features of sandwiched metal-based chalcogenide-related materials have been best revealed lately, including excellent transparency, carrier mobility, superior pliability, and high specific surface area. Layered semi-conducting transition-metal dichalcogenides such as WS₂, MoS₂, SnS₂, and WSe₂ materials have been reported to have exceptional optical and electrical properties, making them ideal for photo sensing applications [5–8].

SnS₂ is a significant optical semiconductor that can be tuned to exhibit either n-type or p-type conductivity based on the dominance of either tin or sulfur molar concentrations [9]. Depending on the bonding properties of tin with sulfur, the sulfide exists in a number of phases, such as SnS, SnS₂,

✉ A. M. S. Arulanantham
amsarul@gmail.com

- ¹ St. Joseph College of Arts and Science, Vaikalipatti, Tirunelveli 627808, India
- ² Department of Physics, Pondicherry University, Pondicherry 605014, India
- ³ Thin Film Research Centre, Kongu Engineering College, Perundurai 638060, India
- ⁴ Department of Physics, School of Science and Humanities, Vel Tech Rangarajan Dr.Sagunthala R&D Institute of Science and Technology, Avadi, Chennai 600062, India
- ⁵ Advanced Functional Materials and Optoelectronic Laboratory (AFMOL), Department of Physics, Faculty of Science, King Khalid University, P.O. Box 9004, Abha, Saudi Arabia

Sn_3S_4 , and Sn_2S_3 [10], where the oxidation number of tin can be II+ and/or IV+, while those of sulfur is II-. Tin disulfide (SnS_2) is one of those semiconductors that had received a considerable attention because of its favorable structural and optical features [11]. Tin disulfide (SnS_2) is a semiconductor having a band gap in the range of 2–3 eV and having a CdI_2 -type structure, composed from SnS_6 interconnected octahedra layers [12, 13]. The photo conductance is caused by its broad band gap [14, 15], which allows it to be used in optoelectronic and solar cell devices [16]. Dielectric materials having an insignificant loss, high dielectric constant and thermal stability are required for microelectronic packaging applications [17–19]. Due to oxygen vacancies, tin disulfide oxide thin films have a very high electron density of 10^{13} cm^{-3} [20]. Due to its photoactive nature, it can also serve as the premier host material for rare earth elements which are optically active. Eu^{3+} ions have excellent luminescence capability in the red spectral region and hence they are the highly preferred dopant among rare earth ions for usage in light emitting devices. Thermo luminescence, photo luminescence, and cathode luminescence characteristics of Eu-doped SnO_2 are all outstanding [21–25].

Chemical vapour deposition (CVD) [26], electron beam induced deposition, spray pyrolysis [27], vacuum evaporation [28], reactive evaporation [29], dip coating [30], and chemical bath deposition [31] are more commonly used to manufacture SnS_2 thin films. Most of the approaches needed to produce an efficient film necessitate either a very high temperature environment or specialized reactors. Every technique used to form a thin film has its own set of benefits and drawbacks. However, researchers are interested in the Spray approach, due to its cost-effectiveness, viability for massive area deposition, and capability of producing homogeneous and well-adhered thin coatings on the substrate. The nebulizer spray pyrolysis (NSP) technique is a very simple, inexpensive and practical alternative to existing thin film synthesis technologies. To our knowledge, no convincing data on the structural, morphological, and opto-electronic characteristics of Eu rare earth ion-doped SnS_2 thin films deposited by the NSP approach are known. A systematic examination of the effect of Eu doping in the SnS_2 thin films using the NSP process has been undertaken in this work. The size of sprayed droplets can be varied to give a smooth-surfaced thin film after optimizing other coating parameters in spray pyrolysis process. The nebulizer spray pyrolysis approach produces a flat surface coating suitable for optoelectronic devices. In the nebulizer spray pyrolysis technology, carrier gas pressure is the most important control parameter for producing a high-quality film. Spray factors such as substrate temperature, solution flow rate, solution concentration, film growth rate, droplet residing time, bulk and surface diffusion processes can all be optimized to enhance the quality and properties of the fabricated thin films.

In the present study, SnS_2 thin films were produced under varied doping concentrations of Eu (0–6 wt%) to improve its optoelectronic capabilities. NSP experimental procedures were used to probe the impact of doping concentration on the inherent properties of SnS_2 thin films. Finally, a SnS_2 thin film-based photodetector device was fabricated with Ag paste as contact electrode (SnS_2/Ag) which demonstrated 97% external quantum efficiency (EQE).

2 Experimental procedures

2.1 SnS_2 films preparation

A nebulizer was used to convert the precursor solution into an aerosol consisting of nozzle-generated micro droplets suspended in air. Europium(III) chloride from Sigma Aldrich with a purity of 99.9% was used as dopant. Tin disulfide thin films doped with different Eu ion concentrations (2, 4 and 6 wt%) were formed on bare glass substrates through nebulizer spray pyrolysis method keeping the substrate temperature constant at 325 °C. Nebulizer spray pyrolysis is a relatively simple and economic method to create SnS_2 -Eu thin films. The initial precursor solution was made utilizing highly purified stannic chloride pentahydrate $\text{SnCl}_4 \cdot 5\text{H}_2\text{O}$ (Sigma Aldrich, 98%), and thiourea (Sigma Aldrich, 99.99%) was dissolved discretely in a mixed solution having isopropyl alcohol and de-ionized water in a ratio 3:1. Tin tetrachloride pentahydrate and thiourea solutions were utilized in the molarity ratio of 1:2. For a thorough dissolution, concentrated hydrochloric acid is added in drops. These two solutions were mixed in equal parts, taken in the pocket nebulizer and sprayed over the glass substrate with the carrier gas pressure set at 1.5 kg/cm². The glass nozzle is fixed at 5 cm above the substrate. The volume of the precursor solution was 10 ml with the solution flow rate set to 0.8 ml/min during spraying. After being deposited, the as synthesized film was enabled to cool until it reaches room temperature.

2.2 Characterization analysis of Eu-doped SnS_2 thin film

Structural analysis of the Eu-doped SnS_2 film was done using XRD spectrum recorded through PAN analytical X' Pert PRO having CuK_α source within a Bragg angle of 10°–80°. The thickness of Eu-doped SnS_2 thin films were studied using Mitutoyo SJ-301 type profilometer. The surface roughness and topology of the grown films were analyzed through an atomic force microscope supplied by ZEISS. An EVO 18 ZEISS model Scanning electron microscope with an energy dispersive X-ray analyzer was utilized with the range of energy from 0.5 to 10 eV to obtain the surface morphology. The optical characteristics were obtained using

a double-beam Lambda Perkin–Elmer UV–Vis–NIR spectrophotometer within the wavelength range of 300–1100 nm. On the point probe hall effect system, the electrical parameters were recorded using Keithley source meter. The samples were illuminated with a 405 nm laser, and the studies were also conducted in the dark at night to eliminate the common electromagnetic wave influence on the Ag scattering within the prepared film. Using a Xenon lamp as a photometer and a Keithley 2450 source meter, the photo-electric responses of the fabricated films were carried out.

3 Results and discussion

3.1 Structural examination of Eu-doped SnS₂ thin film

Figure 1 presents the XRD patterns of pure and Eu-doped SnS₂ films deposited with varying Eu doping ratios (0–6 at %) on the glass substrate maintained at 325 °C. The hexagonal structured single crystal nature of SnS₂ was established from the X-ray diffractograms which agree well with the JCPDS card numbered 23-0677. Regardless of the variation in Eu doping ratio, all the samples exhibited a predominant peak along (001) plane revealing the preferential growth orientation and purity of phase in the grown SnS₂ films. Similar kind of

single-phase crystallite structure was reported for SnS₂, ultrasonic spray technique [32], and chemical method [33]. The peak intensity of the (001) plane is increased proportional to the Eu doping concentration as it was varied from 0 to 2% because of peak width reduction and stress reduction in the deposited films [34]. The observed peak intensity is reduced for 4% and 6% Eu-doped films, which may be attributed to the following reasons: (1) saturation level attained at higher doping concentration, (2) increased crystal defect due to the disorder in adherence of the ions on the substrate. This is due to increase in the number of ions, which do not get enough time and space to adhere on to the substrate and leads to quick precipitation. Moreover, no other peaks corresponding to any other impurity or Europium (Eu)-related crystalline phases were found in X-ray diffractograms. As the radius of Sn⁴⁺ ion (0.69 Å) is lower than the radius of Eu³⁺ ion (0.947 Å), the incorporation of Eu³⁺ as substitution ion for SnS₂ in the lattice, induces significant change in the size of the crystallites and lattice constant. The difference in the valence state of Sn⁴⁺ and Eu³⁺ ion and its adverse effects were reported earlier for Mg-doped SnS₂ [34] and Zn-doped SnS₂ [35]. When the ionic radius of the element doped (Eu³⁺—0.947 Å) is higher than Sn⁴⁺ (0.69 Å) at the interstitial site of SnS₂ crystal lattice, the lattice distance (*d_{hkl}*) of adjacent planes will get increased due to increase in the cell volume [34]. Thus, from Bragg’s law ($n\lambda = 2d_{hkl}\sin\theta$), shifting of XRD peaks towards lower angles of 2θ values, will ascribe the d-spacing to increase [36]. The determined value of thickness of the films with different levels of Eu doping concentration is shown in Table 1. The thickness is observed to increase with increase in Eu doping concentration. The increment in the thickness of the films with increasing Eu doping can be ascribed to the increase in the lattice distance (*d_{hkl}*) between adjacent planes.

The average crystallite size was estimated for the plane (001) by applying Scherer’s equation for the SnS₂ thin film capped with Eu [37, 38]:

$$D = \frac{0.9\lambda}{\beta\cos\theta}, \tag{1}$$

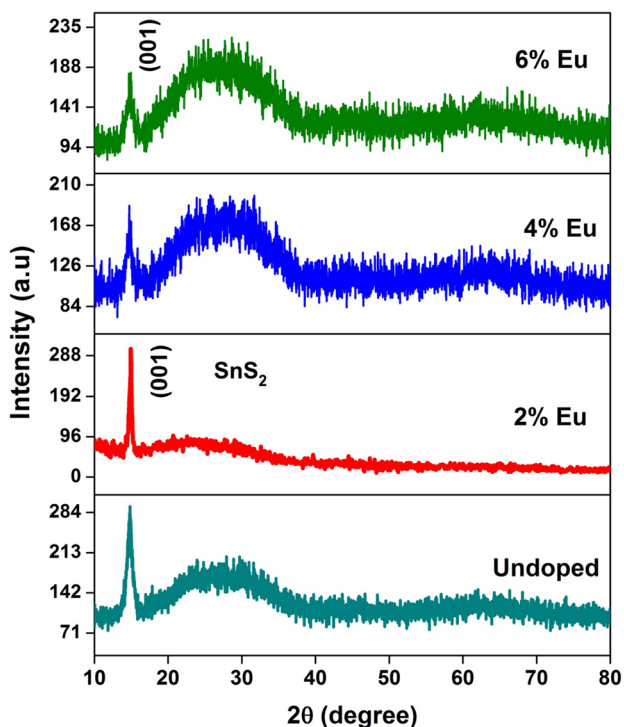


Fig. 1 XRD patterns of undoped and Eu-doped SnS₂ films with different Eu doping contents

Table 1 Micro-structural parameters of undoped and Eu-doped SnS₂ thin films

Eu doping concentration (%)	Thickness (nm)	Crystallite size (nm)	Dislocation density ($\delta \times 10^{15}$ lines/m ²)	Strain ($\epsilon \times 10^{-3}$ /lines ² m ⁴)
0	349	24	1.73	1.82
2	380	32	0.97	0.81
4	428	21	2.26	2.21
6	446	19	2.77	2.68

where λ , β and θ are the wavelength X-ray source, full width at half maxima (FWHM) of the predominant peak and the Bragg diffraction angle, respectively. Using the above formula, the calculated size of the crystallites was found to range between 32 to 19 nm as the Eu doping level is increased from 2 to 6%. The films showed an enhanced crystallinity from 0 to 2%, as the arrangement of atoms is regular in the crystal lattice might be due to the stabilization of the SnS₂ sheet structure for low dopant concentrations. However, when the Eu doping concentration was increased to 4% and 6%, the crystallite size starts decreasing, owing to the increase in the dislocation density and micro strain in the films. This result features the unfavorable effect of higher doping concentration on new nucleation routing to poor crystallinity of the film for 4% and 6% of Eu doping [39, 40]. Variation in crystallite size is due to the expansion of SnS₂ lattice. Similar result was also exposed by Wojcieszak et al. [41].

The more common structural parameters such as micro-strain (ϵ) and dislocation density (δ) were estimated using the below given equations [38, 42]:

$$\epsilon = \frac{\beta \cos \theta}{4} \quad (2)$$

$$\delta = \frac{1}{D^2}. \quad (3)$$

The dislocation density and micro strain values increases gradually as the Eu doping increases from 2 to 6%, as shown in Table 1. The 2% Eu-doped SnS₂ film has a largest crystallite size of 32 nm when compared to other doping concentrations proving the improvement in the crystallinity of the films due to the enhancement in the arrangement of atoms in the regular crystal lattice sites. In addition the increase in the Eu ion concentration from 4 to 6 at%, boosted the dislocation density and micro

strain values. The observed upshots mark the unfavorable effect of increase in doping concentration (> 2 at%) on the crystallinity leading to decline in the quality of the films [42]. Table 2 presents the comparison made on the effect of different dopants on crystallite size, dislocation density and strain.

3.2 Surface morphological studies of Eu-doped SnS₂ film

3.2.1 Eu-doped SnS₂ film surface characteristics using SEM

Figure 2a–d shows the SEM micrographs of Eu-doped SnS₂ films. SEM image present both individual and clustered particles which make the surfaces non-uniform and inhomogeneous. It can be also be seen that, there is no evidence of cracks and pinholes in the films except the film 2a without dopant. Increase of Eu concentration cause a major impact on the morphology of the film surface as can be seen in Fig. 2d for the film with highest dopant concentration. It is noted from Fig. 2a, that the sample grown with 0% doping has crystallites of both rounded and irregular shape, while the SEM micrographs given in Fig. 2b, c for samples prepared at 2% and 4% of Eu doping shows spherical grains with uniform coverage on the glass substrate. The 2% Eu doping showed by Fig. 2b establishes a flat and uniform surface filled with (sub) micronic spherical grains, many of them joining to form bigger agglomerations, and seems to have few very small particles which is quite dissimilar from the films coated at 0% and 4%. The mobility and diffusion of atoms on the film surface were found to be increased at 2% Eu concentration resulting in the development of clusters leading to agglomeration [44]. The amalgamation of agglomerated grains paves way to the formation of larger grains with improved crystallinity as witnessed from XRD analysis. The 6% Eu-doped SnS₂ film in Fig. 2d appears to have small islands of particles. Increase of Eu doping from

Table 2 Influence of different dopants on the structural parameters of SnS₂ thin films

Dopant	Atomic %	Crystallite size (nm)	Dislocation density ($\times 10^{15}$ lines/m ²)	Strain ($\times 10^{-3}$ /lines ² m ⁴)	References
Sb	0	15	4.40	2.30	[32]
	2	17	3.40	2.10	
	4	24	1.70	1.40	
	6	28	1.20	1.20	
	8	15	4.40	2.30	
Nd	0	22	2.06	1.16	[43]
	2	26	1.47	1.02	
	4	28	1.26	0.92	
	6	20	2.51	1.34	
Eu	0	24	1.73	0.18	This work
	2	32	0.97	0.08	
	4	21	2.26	0.22	
	6	19	2.77	0.26	

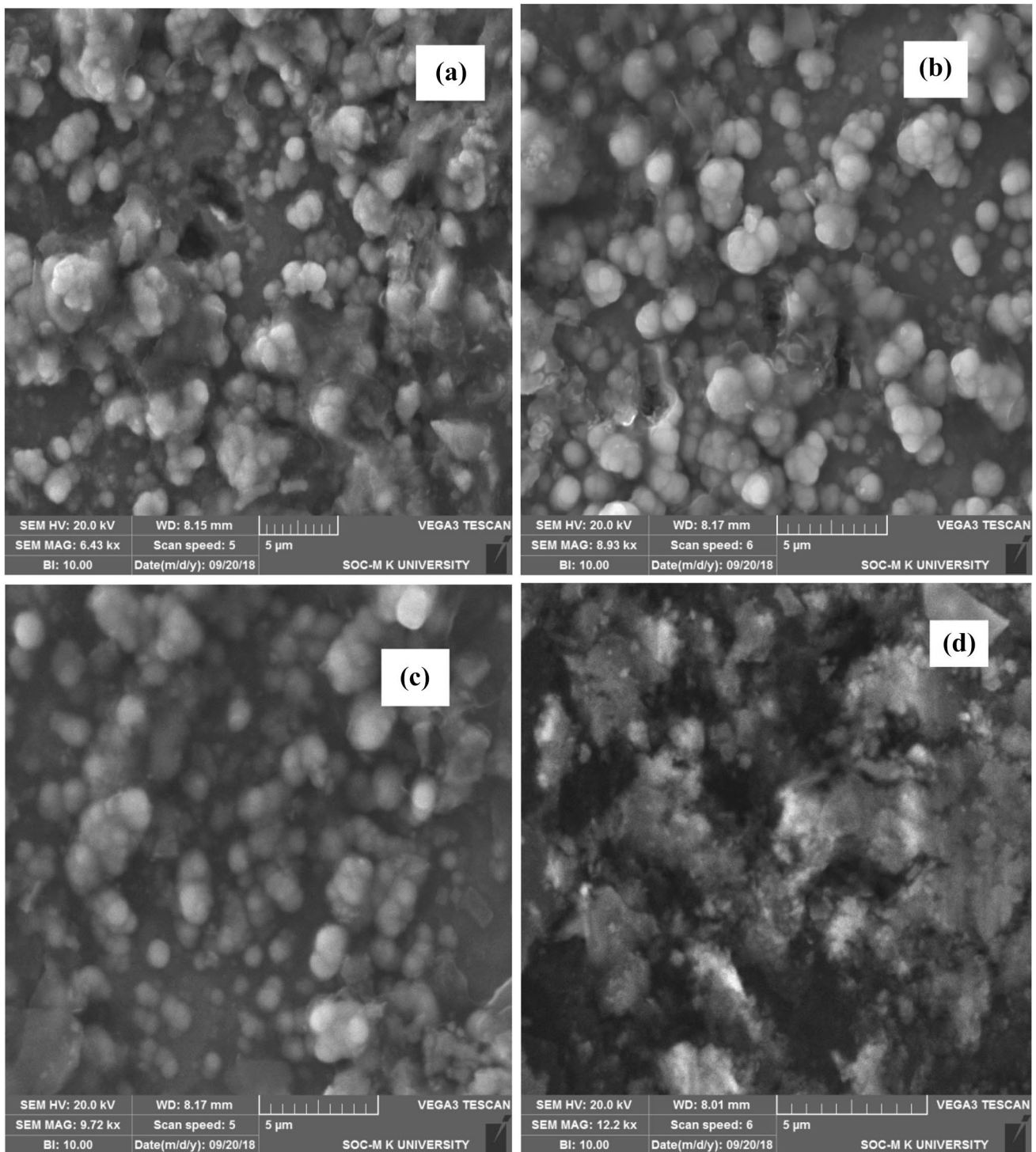


Fig. 2 SEM images of SnS₂ thin films **a** undoped, **b** 2%, **c** 4% and **d** 6% Eu doped SnS₂ films

0 to 2% has increased the size of grains which seems to indicate that relative low levels of Eu doping promotes the grain growth in the films.

3.2.2 EDAX Studies of Eu-doped SnS₂ films

The chemical composition analysis of the Eu-doped SnS₂ thin films deposited through nebulizer spray method was done through EDX spectrum. The EDX spectra of the films

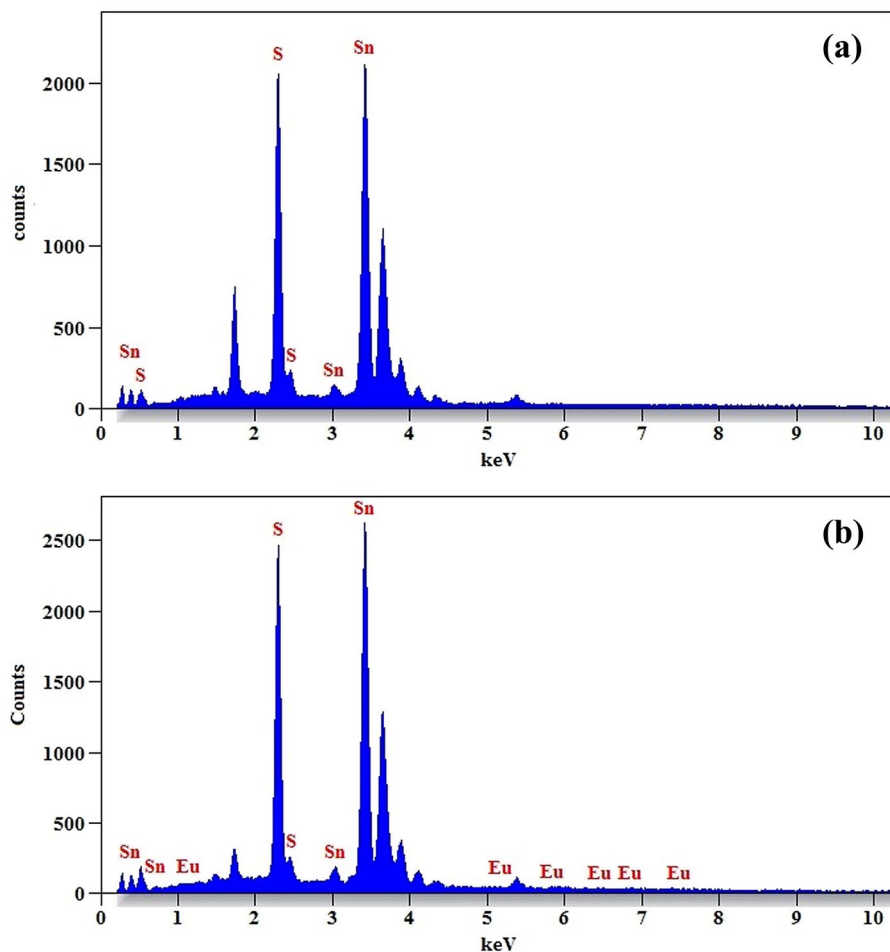
deposited at 0% and 2% of Eu-doping is shown in Fig. 3a, b respectively. The peaks in Fig. 3b clearly confirms the existence of tin (Sn), sulfur (S) and (Eu) Europium in the sample under near stoichiometry with Sn=36.17 and S=59.32 and Eu=2.51 atomic percent. No other additional peaks were found in the EDX spectrum other than Sn, S and Eu peaks.

3.3 AFM analysis of Eu-doped SnS₂ films

From the AFM measurements the surface topographies of a film such as size of grains and surface roughness can be analyzed quantitatively. Figure 4a–d illustrates the 3D AFM images of SnS₂ films for varying Eu concentrations. To acquire the morphological details of the film surface, the prepared films were probed by selecting an area of 2.5 μm × 2.5 μm. The film surface of pure SnS₂ film with 0% doping (Fig. 4a), shows clusters of spherical shaped particles with uniform coverage over the substrate. It is appealing to note that, the SnS₂ films grown with 2% and 4% doping concentration (Fig. 4b, c) presents a distinguishable change in the nucleation of film, indicating an

island-type formation, as a result of the aggregation of smaller grains explained by Volmer–Weber growth mechanism [45]. In addition, it can be seen that increase in the doping concentration increases the grain size. However, when the Eu doping is increased to 6%, it causes a reduction in the grain size. The roughness value of the film is higher for 2% Eu doping. With additional increase in doping concentration to 4% and 6%, the roughness decreased, similar kind of behavior is observed in the earlier report also [46]. The effect of Eu doping on SnS₂ films can be ascertained by the response in the grain size and surface roughness of the deposited films. Dense and more or less of uniform coarse grains with increasing adhesion are found in Eu-doped SnS₂ thin films. The nucleation and the mobility of atoms on the surface get reduced when the Eu doping percentage is less. Hence, adequate doping percentage of atoms must be provided (2% Eu) to combine and create larger grains on the substrates [47] rather than forming islands. It is evident from the AFM analysis that the Eu doping in SnS₂ film has an acceptable effect on the grain size and the surface roughness.

Fig. 3 EDAX spectrum of **a** undoped and **b** 4% Eu doped SnS₂ films



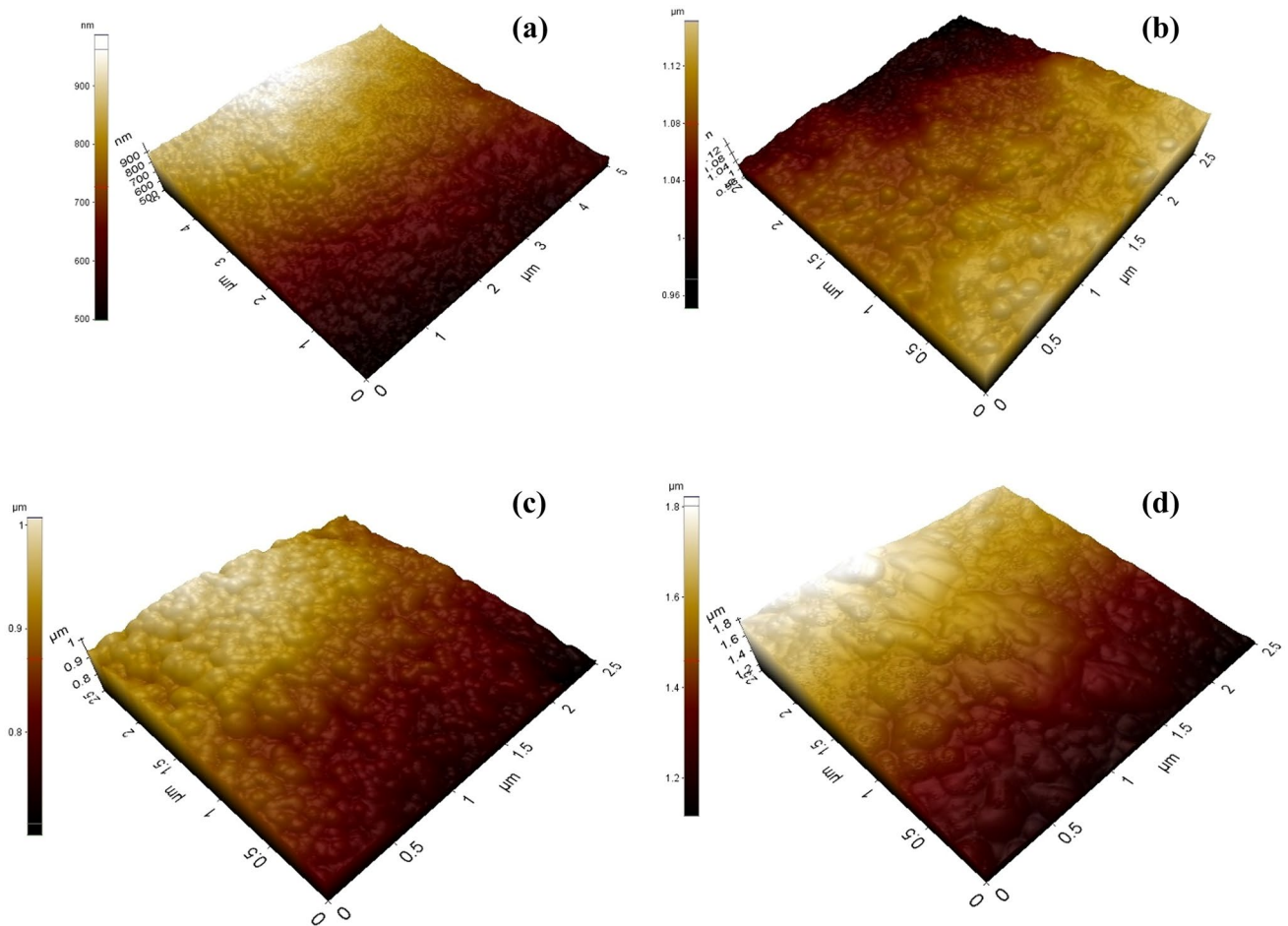


Fig. 4 3D AFM images of a undoped, b 2%, c 4% and d 6% Eu doped SnS₂ films

3.4 Analysis of optical properties

The transmittance (*T*) and absorption coefficient (*A*) plots of Eu-doped SnS₂ thin films with various concentrations are shown in Figs. 5 and 6. As witnessed from Fig. 5, the transmittance of SnS₂ films shows an increase when wavelength is increased up to around 650 nm beyond which the transmittance stays almost constant. When Eu doping concentration is augmented to 4% and 6%, the transmittance is observed to be little less. The surface of the film must be smooth, which is evident from the emergence of multiple interference fringes in the transmittance spectrum. The absorption spectra in Fig. 6 display a rapid decreasing trend in wavelength to 500 nm then it further slowly decreased to 600 nm and remains constant, exhibiting an enhanced crystalline nature of the films. The absorption value increases with escalating the concentration of Eu from 0 to 2%. With further increase in Eu doping concentration from 4 to 6%, the absorption of the film is decreased.

The critical metric that defines the film's absorption capacity and also offers key information about the film's

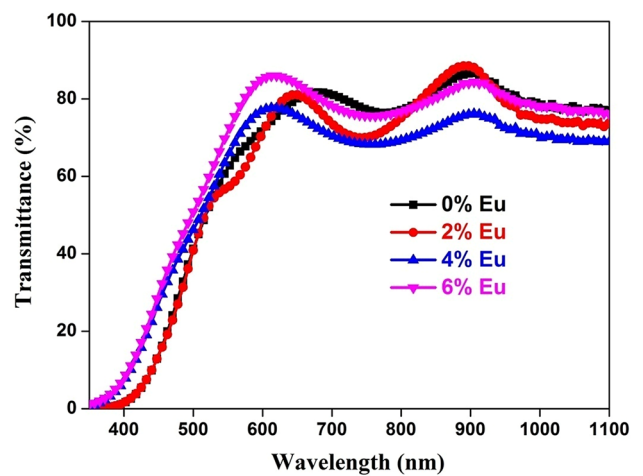


Fig.5 Optical transmittance spectra of Eu-doped SnS₂ thin films

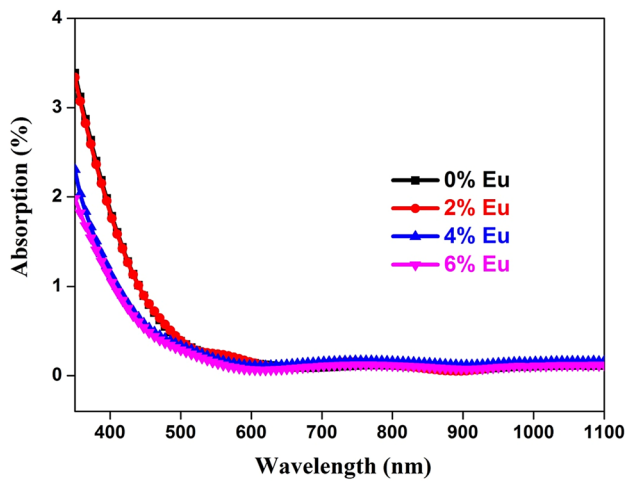


Fig.6 Optical absorbance spectra of Eu-doped SnS₂ thin films

band structure is the absorption coefficient. The following relation [48] was used to calculate the value of ‘ α ’:

$$\alpha = \frac{\text{Film absorbance}}{\text{Film thickness}} \tag{4}$$

For all of the films, the ‘ α ’ value dropped with wavelength, indicating that the films have lower absorption and increased transmittance in the higher wavelength region. With different doping concentrations, the films absorption capacity varies. The value of ‘ α ’ found from the above relation was used to compute the extinction coefficient ‘ k ’ [49]:

$$k = \frac{\alpha \lambda}{4\pi} \tag{5}$$

where α represents absorption coefficient and λ is the wavelength of incident light. When an electromagnetic wave passes through a material, the value of k reflects the degree of attenuation of the wave due to absorption or scattering or both.

The direct bandgap has been calculated from Tauc’s relation [50, 51]:

$$\alpha h\nu = B(h\nu - E_g)^n \tag{6}$$

where $h\nu$ is the energy of incident photon, E_g is the optical bandgap and n is a constant. The plot (Fig. 7) between $(\alpha h\nu)^2$ and $h\nu$ can be used to estimate the value of bandgap of pure and Eu-doped SnS₂ thin films deposited through low cost NSP method. The calculated band gap value increased from 2.70 to 2.91 eV as the concentration of the Eu dopant is varied from 0 to 6%. This increase in bandgap may be rationalized due to: (1) increment in thickness of the films and grain size, (2) variations of localized density of states in the energy gap, (3) change of barrier height at grain boundaries, (4) decrease of strain and increase in lattice constant

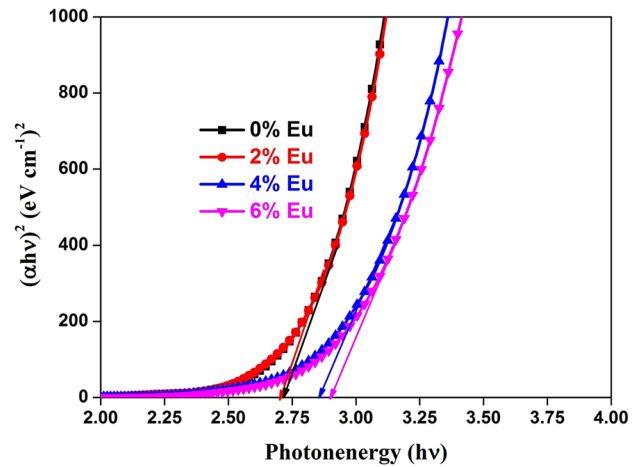


Fig.7 $(\alpha h\nu)^2$ versus $(h\nu)$ plot for Eu-doped SnS₂ thin films

[52] and (5) tight bonding of atoms to each other. When compared to the bulk value (~2.00 eV), the observed band-gap range of the prepared films was found to be relatively higher. The band gap was found to increase up to 2.91 eV, when Eu was made to 6 wt %, which might be due to the change in crystallinity. The observed consequences for the prepared SnS₂ thin films agrees well with the reported direct band gap values utilizing different fabrication methods [53, 54]. The following relation can be used to compute one of the optical constants, refractive index (n) of the prepared SnS₂ thin films [55]:

$$n = \frac{1+R}{1-R} + \left[\left(\frac{1+R}{1-R} \right)^2 - k^2 + 1 \right]^{\frac{1}{2}} \tag{7}$$

where R is the reflectivity and k is the extinction coefficient. Figure 8 shows the change of refractive index (n) and

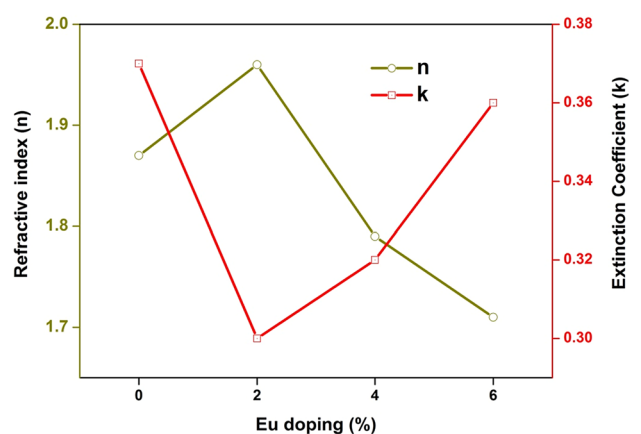


Fig. 8 Refractive index (n) and extinction coefficient (k) of Eu-doped SnS₂ thin films

extinction coefficient (*k*) for various Eu-doped SnS₂ films. The prepared films show a decrease in the refractive index from 1.96 to 1.72 for increasing the Eu doping concentration from 2 to 6%, while the undoped film shows a 1.84 value of refractive index. As evident from the figure, when the concentration of the Eu dopant is increased in limited amount (up to 2%), light propagation through the film will be obstructed because of dense packing of particles, leading to a raise in the value of refractive index [52]. Whereas, the extinction coefficient is found to increase from 0.30 to 0.36 when the Eu doping is increased from 2 to 6%. However, with higher dopant concentration which induces high density of defects, the refractive index decreases and this behavior can be explained by poor packing density similar with the cases of SnS films growth at lower temperatures by chemical bath deposition method [56].

3.5 Electrical Hall measurement in deposited SnS₂ films

Hall effect measurements were performed to compute the carrier density, electrical resistivity and mobility of a semiconductor. The calculated Hall coefficient acknowledges that the films had n-type conductivity. Table 3 summarizes the results of electrical resistivity, mobility, carrier concentration and type of conductivity of SnS₂ thin films prepared at varying Eu doping concentrations as established by Hall Effect probe. The carrier concentration and mobility are considered to be the two main factors that govern the carrier transport properties in semiconductor thin films. In this study, the highest carrier concentration value of $5.43 \times 10^{17} \text{ cm}^{-3}$ and a highest carrier mobility of $3.64 \times 10^2 \text{ cm}^2/\text{Vs}$ was observed for 2% of Eu doping concentration with an associated resistivity of $4.34 \times 10^{-1} \text{ } \Omega \text{ cm}$. The Eu ions act as n-type dopants that increase the amount of free electrons in SnS₂ and thus the conductivity and the Fermi energy of SnS₂ is shifted upward after doping with Eu due to the increase in the amount of oxygen vacancies on the surface of SnS₂, [26] which will result in an increased carrier concentration [57], resulting in reduced resistivity. For 4% of Eu doping, the values of carrier concentration $5.19 \times 10^{15} \text{ cm}^{-3}$, carrier mobility $2.89 \times 10^2 \text{ cm}^2/\text{Vs}$ which were found to decrease and a higher resistivity of $1.18 \times 10^{+1} \text{ } \Omega \text{ cm}$ when compared

to 2% of Eu doping concentration. Further increasing the Eu doping concentration to 6%, the values of carrier concentration, carrier mobility were decreased and resistivity $1.66 \times 10^{+2} \text{ } \Omega \text{ cm}$ was enhanced. This decrement in carrier concentration, carrier mobility and increment in resistivity may be accredited because of the following reasons (1) difference in the ionic radii between Eu³⁺ and Sn⁴⁺, (2) higher doping concentrations (4% and 6%), causing an excess of Eu atoms which leads to the creation of more number of interstitial and point defects in the SnS₂ lattice site leading to an increase in the scattering mechanism by phonon and ionized impurity. Thus, it can be concluded that, as the concentration of Eu dopant increases to an optimum value, higher values of carrier concentration is expected as the doping stimulated charges increases along with the improvement in the size of the crystallites in concordance with the XRD results. Similar kind of behaviour is observed when SnS is doped with bismuth [47] and Ag [58] deposited using spray pyrolysis technique.

3.6 Photosensitivity studies

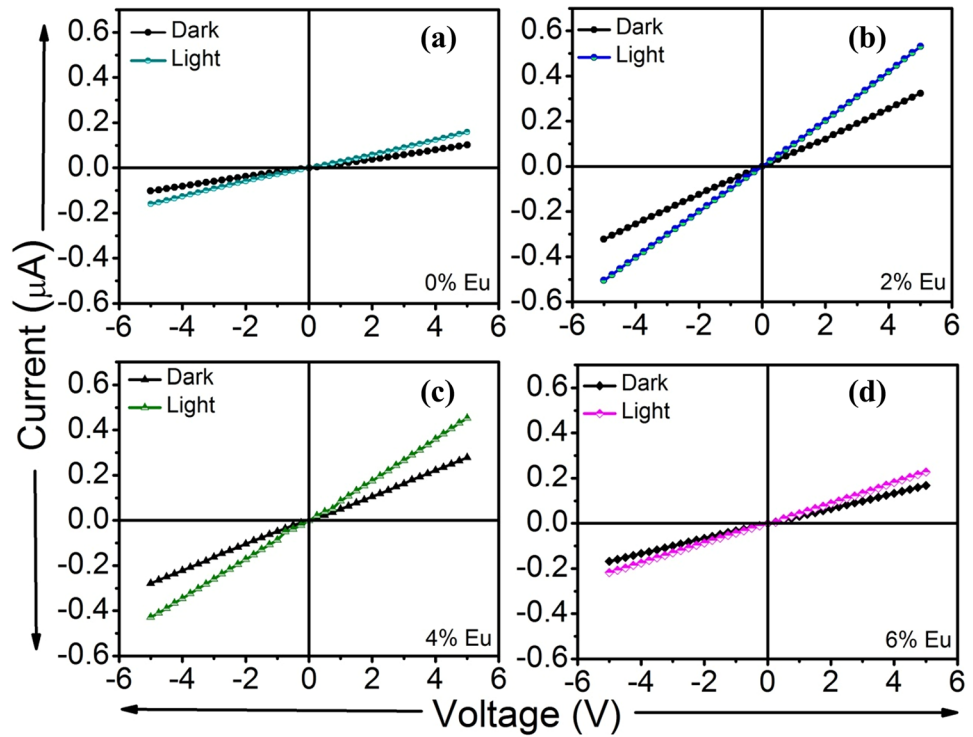
The photosensing capabilities of the produced SnS₂ films were investigated under illumination with 405 nm laser using various power intensities. The manufactured SnS₂ films were endowed with silver paste contact electrodes to make visible radiation photo detectors. Figure 9 depicts the current fluctuation under dark condition and when illuminated with 405 nm laser light vs. bias increasing forward (from 0 to 5 V) and reversed voltage (from 0 to - 5 V). Furthermore, as shown in Fig. 9, the current is marginally increased as the Eu doping concentration (0–2%) is increased. This increase in current value could be due to the improvement in the thickness of the film, grain size, energy band gap, and carrier concentration, as well as a larger light absorbing surface that would result in more photo-generated carriers when exposed to laser light. The above findings are supported by structural, optical, and electrical studies also.

However, 6% of Eu-doped SnS₂ films have lattice defects or sulfur vacancies, as well as poor crystalline quality (as determined by XRD), resulting in a maximum reduction in the current under both light and dark conditions. However, these lattice flaws may help to boost the current level when

Table 3 Electrical properties of Eu-doped SnS₂ thin films

Eu doping concentration (%)	Resistivity ($\Omega \text{ cm}$)	Carrier concentration ($/\text{cm}^3$)	Mobility (cm^2/vs) $\times 10^2$	Type of conductivity
0	$9.32 \times 10^{+1}$	2.80×10^{16}	3.38	N
2	4.34×10^{-1}	5.43×10^{17}	3.64	N
4	$1.18 \times 10^{+1}$	5.19×10^{15}	2.89	N
6	$1.66 \times 10^{+2}$	1.29×10^{15}	2.90	N

Fig. 9 I–V characteristics of **a** undoped, **b** 2%, **c** 4% and **d** 6% Eu doped SnS₂ films



illuminated with light for samples which are moderately doped. The growing/decreasing pattern of light/dark current ($I_{\text{light}}/I_{\text{DC}}$) with increasing forward and reverse bias voltage is shown in Fig. 9. Furthermore, the photocurrent (I_{PC}) of illuminated Eu:SnS₂ films progressively increases with bias voltage, following the same fashion as under dark condition (I_{DC}). $I_{\text{PC}} = I_{\text{light}} - I_{\text{DC}}$ [59], where I_{light} is the current when illuminated with light at 405 nm which is used to calculate the photocurrent (I_{PC}).

3.6.1 The specific detectivity (D^*), external quantum efficiency (EQE) and responsivity (R)

The responsivity (R), detectivity (D^*), and external quantum efficiency (EQE), the three most sought photo-detector parameters, were also investigated. The ratio of photocurrent (I_{p}) to power density (P_{in}) of incident light and area of the detector can be used to compute the responsivity using the formula below:

$$R = \frac{I_{\text{p}}}{P_{\text{in}} \times A} \tag{8}$$

To calculate D^* and EQE from R value, the following formulas were used:

$$\text{EQE} = R \frac{hc}{e\lambda} \tag{9}$$

$$D^* = R \sqrt{\frac{A}{2eI_{\text{DC}}}} \tag{10}$$

where e is the charge of electron, h is Planck’s constant, and c represents velocity of light in vacuum. Figure 10 depicts the changes in R , D^* , and EQE for SnS₂:Eu photodetector. In addition, Fig. 11 represents the photoresponse properties of the Eu:SnS₂ thin films under NIR illumination at various bias voltages. All of the photo-detector properties were observed to gradually rise with the increase in the

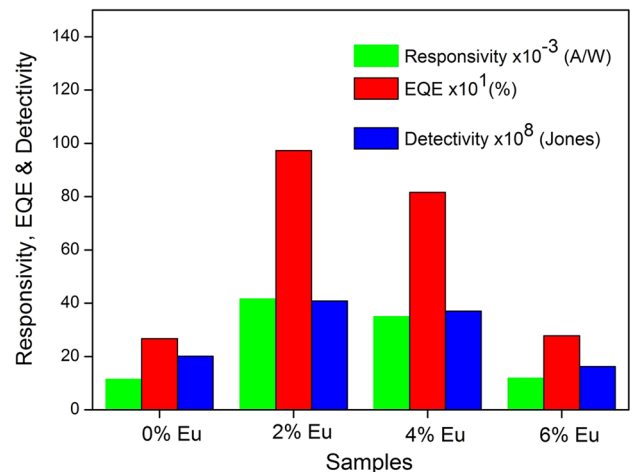


Fig. 10 The differentiations of specific detectivity (D^*), EQE, and responsivity (R) of undoped and Eu doped SnS₂ films

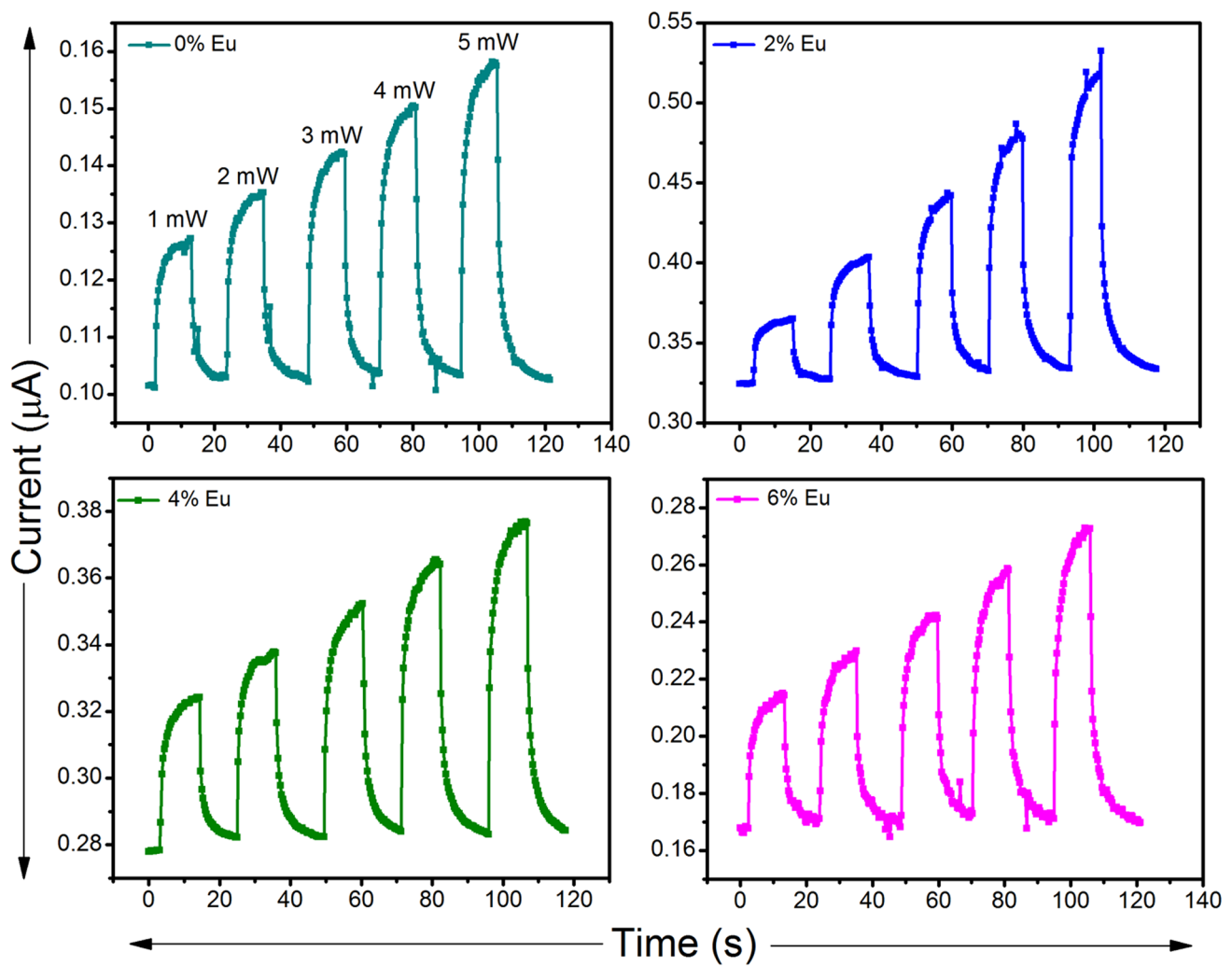


Fig. 11 Photoresponse properties of the Eu:SnS₂ thin films under NIR illumination at various bias voltages

concentration of Eu dopant. For pure SnS₂ to SnS₂:Eu with 2% doping, the R value increases from $11.14 \times 10^{-3} \text{ AW}^{-1}$ to $41.64 \times 10^{-3} \text{ AW}^{-1}$. Furthermore, the R value reduced when the doping concentration was increased, such as 4 and 6% of Eu metal into SnS₂. Reddy et al. [60] recently reported a maximum responsivity value of $0.43 \times 10^{-3} \text{ AW}^{-1}$ for SnS-based detector under light in the visible region. The R value achieved by us for the SnS₂:Eu (2%) detector under same conditions is significantly greater than the reported value. In the prepared SnS₂:Eu detector, this would specify the maximum ratio of I_{DC} and I_p . Furthermore, as shown in Fig. 10, both detectivity and external quantum efficiency values follow the similar trend as R , increasing with increase in the doping concentration and reaches a maximum value for the 2% deposited SnS₂:Eu detector. As a result, the maximum values of D^* and EQE was found to be 40.88×10^8 Jones and 97.24%, respectively, which are substantially improved values for the Eu-doped SnS₂ photo detector. It is worth

mentioning that our D^* for the SnS₂ visible photo detector is larger than the prior result ($D^* = 7.1 \times 10^7$ Jones) [60]. In conclusion, we found that a 2% doped SnS₂:Eu thin film has improved photo-detecting capabilities when compared to pure SnS₂ sample, and is significantly superior to the previously reported results.

3.6.2 Photodetector mechanism

To best learn the mechanism of photocurrent production in Eu-doped SnS₂ detectors, we need to consider the energy band level before and after light irradiation, as shown in Fig. 12. In general, the Ag metal contact work function (4.30 eV) should be closer to the SnS₂ work function (4.81 eV), and it should be greater than the electron affinity of SnS₂ (4.16 eV) for creating ohmic or non-rectifying junctions. Silver (Ag) was chosen as the contact material in this investigation, since it meets all of the criteria.

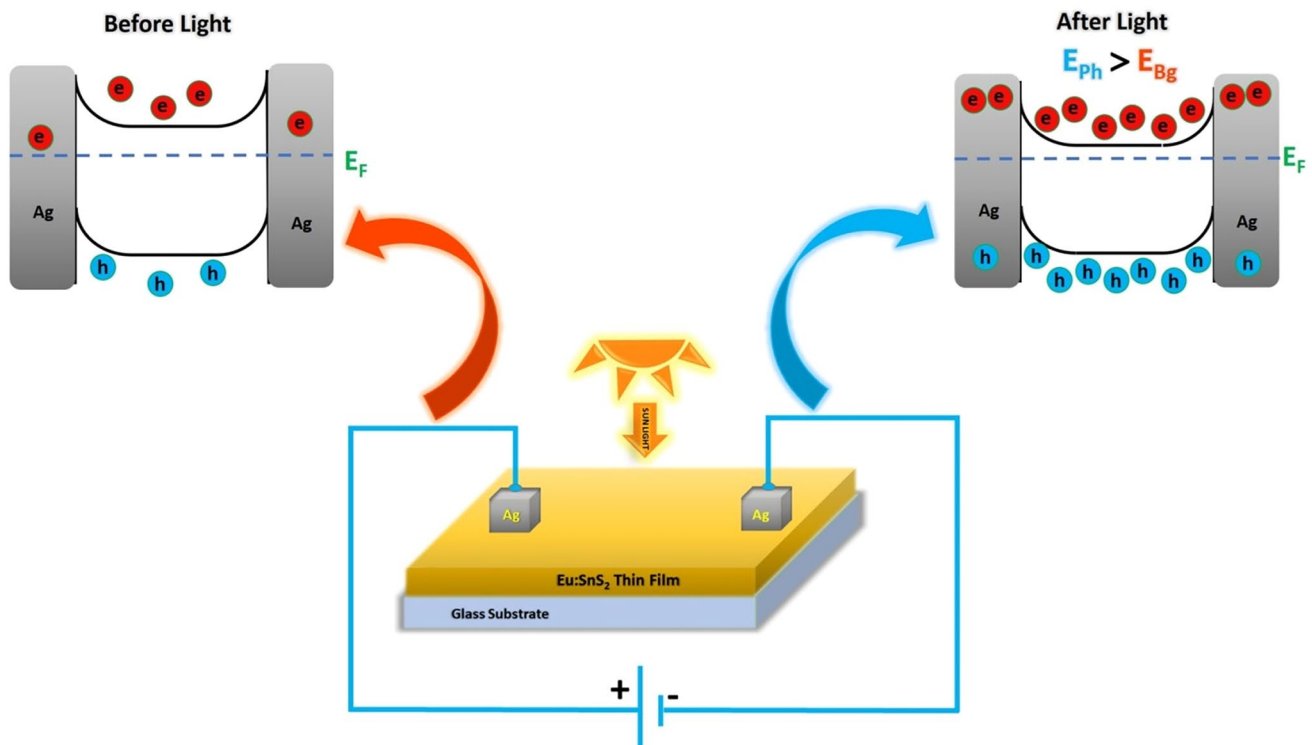


Fig. 12 Schematic representation of Eu doped SnS_2 thin film photo sensing mechanism under dark and light illuminations

Devika et al. [61] investigated the ohmic behavior of metal SnS interfacial structures with various metal contacts ($M = \text{Al, In, Ag, and Sn}$) and discovered that, when compared to other metal SnS interface, the Ag-SnS interface only displayed an Ohmic trend from 0 to 6 V. Ag ions may diffuse into the film during the production of Ag metal contacts on the surface of the film, increasing the net concentration of hole and reducing bending of band at the surface, leading to the formation of ohmic contacts as reported by Jang et al. [62].

In the presence of free electrons, adsorbed oxygen molecules on the surface of the film interact with them to generate ionised oxygen, resulting in the formation of a surface depletion layer [63]. When the energy of the incident photon (3.06 eV) is higher than the optical band gap of Eu:SnS_2 (2.70–2.91 eV) under illumination with visible light (405 nm), the creation of electron–hole pairs increases. These photo-generated electrons could increase the number of carriers in the conduction band, which increases the photocurrent under this circumstance (band-to-band optical excitation). Furthermore, when the Eu-doped SnS_2 film surface is irradiated with a 405 nm laser, the oscillating electrons (hot electrons) can be transferred to a higher energy level, allowing electrons to flow between the Eu:SnS_2 and the metal (Ag) contact. The electron density in the Eu:SnS_2 conduction band increases as a result of this electron transfer. Electron–hole pairs are created and collected at the

Table 4 Photosensitivity properties of Eu-doped SnS_2 thin films

Eu doping concentration (%)	Responsivity ($\text{AW}^{-1}) \times 10^{-3}$	Detectivity ($\times 10^8$ Jones)	External quantum efficiency (EQE) (%)
0	11.44	20.12	26.7
2	41.64	40.88	97.24
4	18.24	25.86	56.24
6	11.90	16.25	27.80

electrodes when highenergy photon is allowed to illuminate the surface of the semiconducting film (Table 4).

4 Conclusions

The NSP process was used to successfully generate $\text{SnS}_2:\text{Eu}$ thin films with different doping concentrations from pure to 6% Eu doping for photo-detector applications. From the structural characterization of the prepared thin films, the pure SnS_2 samples were ascertained to have hexagonal structure and an increased crystallinity was observed when SnS_2 is doped with 2% Eu, whereas at higher doping levels (4 and 6%) it diminished due to the increasing of defects number. The $\text{SnS}_2:\text{Eu}$ thin films have a consistent 2-D spherical grains, according to morphological investigation. The

optical measurements revealed that the SnS₂:Eu sample doped at 2% had a higher absorption and a lower bandgap value of 2.72 eV. According to the photo-sensing results, the 2% SnS₂:Eu thin film photo-detector had a higher responsivity, external quantum efficiency, and detectivity values of $41.64 \times 10^{-3} \text{ AW}^{-1}$, 97.24% and 40.88×10^8 Jones, respectively. The obtained results indicated that SnS₂:Eu thin films could be used in photo-detector applications. This work reveals that SnS₂:Eu is a potential choice for visible area photo detector and nebulizer assisted spray pyrolysis is an ideal technique for the fabrication of sophisticated and integrated thin film-based semiconductor devices, as well as providing a reasonable and economic synthesis approach for producing metal chalcogenide thin films.

Acknowledgements The authors from KKU express their appreciation to the Deanship of Scientific Research at King Khalid University, for funding this work through the research groups program under Deanship of Scientific Research, King Saud University, Grant number R.G.P.2/112/41.

Declarations

Conflict of interest No conflicts of interests exist between the authors.

References

- M. Afzaal, P. O'Brien, Recent developments in II–VI and III–VI semiconductors and their applications in solar cells. *J. Mater. Chem.* **16**, 1597–1602 (2006)
- S. VaradharajaPerumal, D. Alagarasan, R. Ganesan, M.N. Satyanarayan, G. Hegde, Controlled growth of 1D-ZnO nanotubes using one-step hot plate technique for CZTS heterojunction solar cells. *Mater. Sci. Semicond. Process.* **106**, 104763 (2020)
- A. Bafekry, M. Shahrokhi, A. Shafique, H.R. Jappor, M.M. Fadlallah, C. Stampfl, M. Ghergherehchi, M. Mushtaq, S.A. Hossein-Feghhi, D. Gogova, Semiconducting chalcogenide alloys based on the (Ge, Sn, Pb) (S, Se, Te) formula with outstanding properties: a first-principles calculation study. *ACS Omega* **6**(14), 9433–9441 (2021)
- S. Roychowdhury, M. Samanta, S. Perumal, K. Biswas, Germanium chalcogenide thermoelectrics: electronic structure modulation and low lattice thermal conductivity. *Chem. Mater.* **30**, 5799–5813 (2018)
- J. Li, C. Nie, F. Sun, L. Tang, Z. Zhang, J. Zhang, Y. Zhao, J. Shen, S. Feng, H. Shi, X. Wei, Enhancement of the photo response of monolayer MoS₂ photodetectors induced by a nanoparticle grating. *ACS Appl. Mater. Interfaces* **12**, 8429–8436 (2020)
- T.H. Tsai, Z.Y. Liang, Y.C. Lin, C.C. Wang, K.I. Lin, K. Suenaga, P.W. Chiu, Photo gating WS₂ photodetectors using embedded WSe₂ charge puddles. *ACS Nano* **14**, 4559–4566 (2020)
- J. Chen, Q. Wang, Y. Sheng, G. Cao, P. Yang, Y. Shan, F. Liao, Z. Muhammad, W. Bao, L. Hu, R. Liu, C. Cong, Z.J. Qiu, High-performance WSe₂ photodetector based on a laser-induced p-n Junction. *ACS Appl. Mater. Interfaces* **11**, 43330–43336 (2019)
- S. Das, K.J. Sarkar, B. Pal, H. Mondal, S. Pal, R. Basori, P. Banerji, SnS₂/Si nanowire vertical heterostructure for high performance ultra-low power broadband photodetector with excellent detectivity. *J. Appl. Phys.* **129**, 53105–53112 (2021)
- S.Y. Cheng, G.N. Chen, Y. Chen et al., Structure and properties of SnS films prepared by electro-deposition in presence of EDTA. *Opt. Mater.* **29**, 439 (2006)
- T. Jiang, G.A. Ozin, New directions in tin sulfide materials chemistry. *J. Mater. Chem.* **8**, 1099–1108 (1998)
- C. Julien, M. Eddreif, I. Samaras, M. Balkanski, Resonant Raman scattering studies of SnS₂ crystals. *Mater. Sci. Eng. B* **15**, 70 (1992)
- Y.T. Qien, *Introduction to Crystal Chemistry*, vol. 280, 2nd edn. (Press of University of Science and Technology of China, Hefei, 1999)
- G. Domingo, R.S. Itoga, C.R. Cannewurf, Fundamental optical absorption in SnS₂ and SnSe₂. *Phys. Rev.* **143**, 536 (1966)
- S. Polarz, B. Smarsly, C. Goltner, M. Antonietti, The interplay of colloidal organization and oxo cluster chemistry: polyoxometalate-silica hybrids—materials with a nano chemical function. *Adv. Matter.* **12**, 1503 (2000)
- M.J. Lanzafame, J. Michael, Synthesis of SnS₂ nanocrystals via a solvothermal process. *Diss. Abstr. Int. B* **54**(1), 263 (1993)
- J. Morales, V.C. Perez, J. Santos, L.J. Tirado, Ultra-high vacuum deposition of Na on SnS₂ in single crystal and powder forms: evidence of a decomposition reaction. *J. Electrochem. Soc.* **143**(a), 2847 (1996)
- G. Wu, Y. Cheng, K. Wang, Y. Wang, A. Feng, Fabrication and characterization of OMMT/BMI/CE composites with low dielectric properties and high thermal stability for electronic packaging. *J. Mater. Sci.* **27**, 5592–5599 (2016)
- G. Wu, Y. Cheng, Y. Ren, Y. Wang, Z. Wang, H. Wu, Synthesis and characterization of γ -Fe₂O₃@ C nanorod-carbon sphere composite and its application as microwave absorbing material. *J. Alloys Compd.* **652**, 346–350 (2015)
- G. Wu, J. Li, K. Wang, Y. Wang, C. Pan, A. Feng, In situ synthesis and preparation of TiO₂/polyimide composite containing phenolphthalein functional group. *J. Mater. Sci. Mater. Electron.* **28**, 6544–6551 (2017)
- A.M.S. Arulanantham, S. Valanarasu, S. Rex Rosario, A. Kathalingam, M. Shkir, V. Ganesh, I.S. Yahia, Nebulizer spray assisted chemical vapour deposited (NACVD) tin disulfide (SnS₂) thin films for solar cell window layer applications. *Mater. Res. Express* **6**(9), 096422 (2019)
- D.F. Crabtree, The luminescence of SnO₂-Eu₃. *J. Phys. D Appl. Phys.* **8**(1), 107–116 (1975)
- D.F. Crabtree, Luminescence and charge compensation in SnO₂ doped with rare earth ions. *J. Phys. D Appl. Phys.* **11**(11), 1543–1551 (1978)
- G. Wang, Y. Yang, Q. Mu, Y. Wang, Preparation and optical properties of Eu³⁺-doped tin oxide nanoparticles. *J. Alloys Compd.* **498**(1), 81–87 (2010)
- E.A. Morais, L.V.A. Scalvi, L.P. Ravaro, S.M. Li, E.A. Floriano, Optical and transport properties of rare-earth trivalent ions located at different sites in sol–gel SnO₂. *J. Phys. Conf. Ser.* **249**, 012005 (2010)
- J. Chen, J. Wang, F. Zhang, D. Yan, G. Zhang, R. Zhuo, P. Yan, Structure and photoluminescence property of Eu-doped SnO₂ nanocrystalline powders fabricated by sol–gel calcination process. *J. Phys. D Appl. Phys.* **41**(10), 105306 (2008)
- L.S. Price, I.P. Parkin, A.M.E. Handy, R.J.H. Clark, Atmospheric pressure chemical vapor deposition of tin sulfides (SnS, Sn₂S₃, and SnS₂) on glass. *Chem. Mater.* **11**, 1792–1799 (1999)
- A. Ortiz, S. Lopez, Spray pyrolysis deposition of Sn_xS_y thin films. *Semicond. Sci. Technol.* **9**, 2130 (1994)
- K.W. Nnebesney, G.E. Collins, P.A. Lee, L.K. Chau, J. Danziger, E. Osburn, N.R. Armstrong, Structural, morphological and optical properties of SnS₂ thin films by nebulized spray pyrolysis technique. *Chem. Mater.* **3**, 829 (1991)

29. J. George, K.S. Joseph, Absorption edge measurements in tin disulphide thin films. *J. Phys. D* **15**, 1109–1116 (1982)
30. C.D. Lokhande, A chemical method for tin disulphide thin film deposition. *J. Phys. D* **23**, 1703 (1990)
31. S.K. Panda, A. Antonakos, Optical properties of nanocrystalline SnS₂ thin films. *Mater. Res. Bull.* **42**, 576 (2007)
32. I.B. Kherchachi, H. Saidi, A. Attaf, N. Attaf, A. Bouhdjar, H. Bendjidi, Y. Benkhetta, R. Azizi, M. Jlassi, Influence of solution flow rate on the properties of SnS₂ films prepared by ultrasonic spray. *Optik* **127**, 4043–4046 (2016)
33. S.K. Panda, A. Antonakos, E. Liarokapis, S. Bhattacharya, S. Chaudhuri, Optical properties of nanocrystalline SnS₂ thin films. *Mater. Res. Bull.* **42**, 576–583 (2007)
34. S. Al-Shomar, Investigation the effect of doping concentration in Ruthenium-doped TiO₂ thin films for solar cells and sensors applications. *Mater. Res. Express.* **7**(3), 036409 (2020)
35. R. Etefagh, N. Shahtahmassebi, M.R. Benam, M.M. BagheriMoghheghi, Effect of Zn doping on optical properties and photoconductivity of SnS₂ nanocrystalline thin films. *Indian J. Phys.* **88**(6), 563–570 (2014)
36. H. Kafashan, R. Ebrahimi-Kahrizsangi, F. Jamali-Sheini, R. Yousefi, Effect of Al doping on the structural and optical properties of electrodeposited SnS thin films. *Phys. Status Solidi A* **213**, 1302–1308 (2016)
37. Y. Jing, X. Cheng-Yan, Y. Li, F. Zhou, X.S. Chen, H. Ping-An, L. Zhen, Ternary SnS_{2-x}Se_x alloys nanosheets and nanosheet assemblies with tunable chemical compositions and band gaps for photodetector applications. *Sci. Rep.* **5**, 17109 (2016)
38. K.D.A. Kumar, S. Valanarasu, V. Tamilnayagam, L. Amalraj, Structural, morphological and optical properties of SnS₂ thin films by nebulized spray pyrolysis technique. *J. Mater. Sci.* **28**(19), 14209–14216 (2017)
39. K. Santhosh Kumar, A. GowriManohari, C. Lou, T. Mahalingam, S. Dhanapandian, Influence of Cu dopant on the optical and electrical properties of spray deposited tin sulphide thin films. *Vacuum* **128**, 226 (2016)
40. A. Bokare, A. Sanap, M. Pai, S. Sabharwal, A.A. Athawale, Antibacterial activities of Nd doped and Ag coated TiO₂ nanoparticles under solar light irradiation. *Colloids Surf B Bio Interfaces.* **102**, 273 (2013)
41. D. Wojcieszak, M. Mazur, M. Kurnatowska, D. Kaczmarek, J. Domaradzki, L. Kepinski, K. Chojnacki, Influence of Nd-doping on photocatalytic properties of TiO₂ nanoparticles and thin film coatings. *Int J Photo Energy.* **2014**, 1–10(2014)
42. N. Farhad, J.-S. Farid, Y. Ramin, Photocurrent properties of undoped and Pb-doped SnS nano structures grown using electro-deposition method. *J. Electron. Mater.* **44**(12), 4734 (2015)
43. N. Anitha, M. Anitha, K. Saravanakumar, S. Valanarasu, L. Amalraj, Fabrication of antimony doped tin disulfide thin films by an inexpensive, modified spray pyrolysis technique using nebulizer. *J. Phys. Chem. Solids* **119**, 9–18 (2018)
44. T. Sall, M. Mollar, B. Mari, Substrate influences on the properties of SnS thin films deposited by chemical spray pyrolysis technique for photovoltaic applications. *J. Mater. Sci.* **51**(16), 7607–7613 (2016)
45. V. An, M. Dronova, A. Zakharov, Optical and AFM studies on p-SnS thin films deposited by magnetron sputtering. *Chalcogenide Lett.* **12**, 483–487 (2015)
46. T.S. Reddy, M.S. Kumar, Co-evaporated SnS thin films for visible light photodetector applications. *RSC Adv.* **6**(98), 95680–95692 (2016)
47. A.G. Manohari, S. Dhanapandian, C. Manoharan, K.S. Kumar, T. Mahalingam, Physical properties of spray pyrolyzed Ag-doped SnS thin films for opto-electronic applications. *Mater. Sci. Semicond. Process.* **17**, 138–142 (2014)
48. A.A. Al-Ghamdi, S.A. Khan, S. Al-Heniti, F.A. Al-Agel, T. Al-Harbi, M. Zulfeqar, Effects of laser irradiation on optical properties of amorphous and annealed Ga₁₅Se₈₁In₄ and Ga₁₅Se₇₉In₆ chalcogenide thin films. *J. Alloys Compd.* **505**, 229–234 (2010)
49. M. Behera, R. Naik, C. Sripan, R. Ganesan, N.C. Mishra, Influence of Bi content on linear and nonlinear optical properties of As₄₀Se_{60-x}Bi_x chalcogenide thin films. *Curr. Appl. Phys.* **19**, 884–893 (2019)
50. H.R. Chandrasekhar, D.G. Mead, Long-wavelength phonons in mixed-valence semiconductor, Sn^{II}Sn^{IV}S₃. *Phys. Rev. B.* **19**, 932–937 (1979)
51. J. Tauc, *Amorphous and Liquid Semiconductors*, 171 (Plenum Press, Boston, 1974)
52. S. Gedi, V.R.M. Reddy, C. Park, J. Chan-Wook, R. Reddy, Comprehensive optical studies on SnS layers synthesized by chemical bath deposition. *Opt. Mater.* **42**, 468–475 (2015)
53. H.L. Zhuang, R.G. Hennig, Theoretical perspective of photocatalytic properties of single-layer SnS. *J. Phys. Rev. B* **88**, 115314 (2013)
54. K.T.R. Reddy, G. Sreedevi, R.W. Miles, Single phase, large grain, p-conductivity-type SnS layers produced using the thermal evaporation method. *J. Mater. Sci. Eng.* **A3**(3A), 182–186 (2013)
55. I.B. Kherchachi, H. Saidi, A. Attaf, N. Attaf, A. Bouhdjar, H. Bendjidi, Y. Benkhetta, R. Azizi, M. Jlassi, The synthesis, characterization and phase stability of tin sulfides (SnS₂, SnS and Sn₂S₃) films deposited by ultrasonic spray. *Optik* **127**, 4043–4046 (2016)
56. S. Gedi, V. Reddy, M. Reddy, C. Park, J. Chan-Wook, K.T. Ramakrishna Reddy, Comprehensive optical studies on SnS layers synthesized by chemical bath deposition. *Opt. Mater.* **42**, 468–475 (2015)
57. X. Zhe, W. Jihuai, W. Tongyue, Q. Bao, X. He, Z. Lan, J. Lin, M. Huang, Y. Huang, L. Fan, Tuning the Fermi level of TiO₂ electron transport layer through europium doping for highly efficient perovskite solar cells. *Energy Technol.* **5**, 1820–1826 (2017)
58. K.S. Kumar, A.G. Manohari, S. Dhanapandian, T. Mahalingam, Physical properties of spray pyrolyzed Ag-doped SnS thin films for opto-electronic applications. *Mater. Lett.* **131**, 167–170 (2014)
59. B. Murali, S.B. Krupanidhi, Facile synthesis of Cu₂CoSnS₄ nanoparticles exhibiting red-edge-effect: application in hybrid photonic devices. *J. Appl. Phys.* **114**(114), 144312 (2013)
60. T.S. Reddy, M.C. Santhosh Kumar, Co-evaporated SnS thin films for visible light photodetector applications. *RSC Adv.* **6**, 95680–95692 (2016)
61. M. Devika, N. Koteeswara Reddy, F. Patolsky, K.R. Gunasekhar, Ohmic contacts to SnS films: selection and estimation of thermal stability. *J. Appl. Phys.* **104**, 124503 (2008)
62. H.W. Jang, J.L. Lee, Mechanism for ohmic contact formation of Ni/Ag contacts on p-type GaN. *Appl. Phys. Lett.* **85**, 24 (2004)
63. K.V. Sopiha, O.I. Malyi, C. Persson, Wu. Ping, *ACS Appl. Mater. Interfaces* **13**(28), 33664–33676 (2021)

Publisher's Note Springer Nature remains neutral with regard to jurisdictional claims in published maps and institutional affiliations.